Eur. Phys. J. B **72**, 509–520 (2009)
DOI: 10.1140/epjb/e2009-00383-0

THE EUROPEAN PHYSICAL JOURNAL B

Regular Article

A universal Hamiltonian for motion and merging of Dirac points in a two-dimensional crystal

G. Montambaux[a], F. Piéchon, J.-N. Fuchs, and M.O. Goerbig

Laboratoire de Physique des Solides, CNRS UMR 8502, Université Paris-Sud, 91405 Orsay, France

Received 17 July 2009
Published online 7 November 2009 –

Abstract. We propose a simple Hamiltonian to describe the motion and the merging of Dirac points in the electronic spectrum of two-dimensional electrons. This merging is a topological transition which separates a semi-metallic phase with two Dirac cones from an insulating phase with a gap. We calculate the density of states and the specific heat. The spectrum in a magnetic field B is related to the resolution of a Schrödinger equation in a double well potential. The Landau levels obey the general scaling law $\epsilon_n \propto B^{2/3} f_n(\Delta/B^{2/3})$, and they evolve continuously from a $\sqrt{nB}$ to a linear $(n+1/2)B$ dependence, with a $[(n+1/2)B]^{2/3}$ dependence at the transition. The spectrum in the vicinity of the topological transition is very well described by a semiclassical quantization rule. This model describes *continuously* the coupling between valleys associated with the two Dirac points, when approaching the transition. It is applied to the tight-binding model of graphene and its generalization when one hopping parameter is varied. It remarkably reproduces the low field part of the Rammal-Hofstadter spectrum for the honeycomb lattice.

PACS. 73.00.00 Electronic structure and electrical properties of surfaces, interfaces, thin films, and low-dimensional structures – 71.70.Di Landau levels – 81.05.Uw Carbon, diamond, graphite – 67.85.-d Ultracold gases, trapped gases

1 Introduction

The main interest of graphene from the fundamental point of view is that the low energy electronic spectrum (around the band center $\epsilon = 0$) is linear, exhibiting the so-called Dirac spectrum around two special points $\boldsymbol{K}$ and $\boldsymbol{K}'$ at the corner of the Brillouin zone (BZ) [1]. As a consequence, the density of states varies linearly with energy. In a magnetic field B, the energy levels around $\epsilon = 0$ vary as $\epsilon_n(B) \propto \sqrt{nB}$, with a two-fold degeneracy corresponding to the two valleys near $\boldsymbol{K}$ and $\boldsymbol{K}'$. The considerable development of research on graphene is partly due to this unusual spectrum [2].

The electronic spectrum of graphene is very well described by a tight binding model on a honeycomb lattice, with three equal couplings t between nearest neighbors [1]. It has been soon realized that, by varying these hopping parameters, new interesting physics could emerge, in particular the existence of a topological transition separating a metallic phase with two Dirac points and an insulating phase with a gap [3–9]. When only one of the three hopping parameters is modified (t', see Fig. 11), the transition occurs when $t' = 2t$. This model that we will call the $t-t'$ model is generic and contains the essential physics of the more general case when the three hopping integrals are different.

Although such variation of hopping parameters may not be feasible in graphene, a transition could well be observed in other systems like the organic conductor $\alpha - (BEDT - TTF)_2 I_3$ [10–12] or an artificial lattice of cold atoms [13–16], where the motion of Dirac points may be induced by changing the intensity of the laser fields.

The spectrum in a magnetic field of the honeycomb lattice has been first considered at low field by McClure [17] who found a $\sqrt{nB}$ dependence of the energy levels near the band center, and R. Rammal calculated the so-called "Hofstadter" spectrum which describes the fractal broadening of the Landau levels, due the the competition between magnetic field and lattice effects [18,19] More recently the Hofstadter-Rammal spectrum has been studied when hopping parameters are modified [20], and it was found that at the topological transition the low field spectrum exhibits a new dependence with the magnetic field of the form $[(n+1/2)B]^{2/3}$ [4]. This is due to the peculiar character of the dispersion relation at the transition: it is linear in one direction and quadratic in the other one. Quite recently it has been proposed that such a hybrid spectrum and the subsequent structure of the Landau levels may exist in VO_2/TiO_2 nanostructures. Note that this system explicitly breaks time-reversal symmetry [21].

[a] e-mail: montambaux@lps.u-psud.fr

In a recent paper, we have studied under which general conditions a pair of Dirac points in the electronic spectrum of a two-dimensional crystal merges into a single point at the topological transition [7]. We have derived a low energy Hamiltonian that describes the physical properties near the transition. The present paper considers in detail these physical properties. The main interest of this work is to present the simplest model which continuously describes the merging of two Dirac points and the subsequent gap opening, and to calculate several physical properties in the vicinity of the transition. We wish to stress that the interest of this work is not only to tune continuously the coupling between two Dirac valleys, but also to study the combination between two distinct and quite interesting dispersion relations: the linear dispersion relation and a dispersion relation with a saddle point. Indeed, the two Dirac points are always separated by a saddle point, and the merging of Dirac points is obviously accompanied by the merging with the saddle point. At this merging, a linear density of states characteristic of the Dirac point approaches a logarithmic density of states characteristic of a saddle point (in $2D$).

The paper is organized as follows. In the next section, we consider a general tight binding problem in $2D$, with two atoms per unit cell and study under which general conditions Dirac points may merge. In Section 3, we study several properties of this Hamiltonian. In particular, we relate the Landau level spectrum to a one-dimensional double well problem, where the two wells correspond to the two valleys around the Dirac points. When approaching the transition, the potential barrier vanishes and the potential becomes quartic at the transition. In Section 4, we show how to relate the parameters of the universal Hamiltonian to the parameters t and t' of the tight binding model on the honeycomb lattice, the so-called $t-t'$ model. In this way, we reproduce with a very good accuracy the low field part of the butterfly spectrum and the lifting of the valley degeneracy of the Landau levels.

2 Construction of the universal Hamiltonian

We consider a two-band Hamiltonian for a $2D$ crystal with two atoms A and B per unit cell. This two-band Hamiltonian is naturally given in terms of the 2×2 matrix

$$\mathcal{H}(\boldsymbol{k}) = \begin{pmatrix} h_{AA}(\boldsymbol{k}) & h_{AB}(\boldsymbol{k}) \\ h_{BA}(\boldsymbol{k}) & h_{BB}(\boldsymbol{k}) \end{pmatrix},$$

with the 2D wave vector $\boldsymbol{k}$. Time-reversal symmetry ($\mathcal{H}(\boldsymbol{k}) = \mathcal{H}^*(-\boldsymbol{k})$) imposes $h_{AB}(\boldsymbol{k}) = {h_{BA}}^*(\boldsymbol{k}) \equiv f(\boldsymbol{k})$ and, together with hermiticity, real symmetric diagonal terms $h_{AA}(\boldsymbol{k}) = h_{AA}(-\boldsymbol{k})$ ($h_{BB}(\boldsymbol{k}) = h_{BB}(-\boldsymbol{k})$). Furthermore, we consider a 2D lattice with inversion symmetry such that $h_{AA}(\boldsymbol{k}) = h_{BB}(\boldsymbol{k})$. The resulting energy dispersion reads $\epsilon_\pm(\boldsymbol{k}) = h_{AA}(\boldsymbol{k}) \pm |f(\boldsymbol{k})|$, and we will even set $h_{AA}(\boldsymbol{k}) = 0$ because this term simply shifts the energy as a function of the wave vector but does not affect the topological properties of the semi-metal-insulator phase transition discussed below.

We, therefore, discuss from now on the Hamiltonian in its reduced form

$$\mathcal{H}(\boldsymbol{k}) = \begin{pmatrix} 0 & f(\boldsymbol{k}) \\ f^*(\boldsymbol{k}) & 0 \end{pmatrix}, \tag{1}$$

where the off-diagonal terms have the periodicity of the Bravais lattice and may be written quite generally in the form:

$$f(\boldsymbol{k}) = \sum_{m,n} t_{mn} e^{-i\boldsymbol{k}\cdot\boldsymbol{R}_{mn}}, \tag{2}$$

where the t_{mn}'s are real, a consequence of time-reversal symmetry $\mathcal{H}(\boldsymbol{k}) = \mathcal{H}^*(-\boldsymbol{k})$, and $\boldsymbol{R}_{mn} = m\boldsymbol{a}_1 + n\boldsymbol{a}_2$ are vectors of the underlying Bravais lattice.

The energy spectrum is given by $\epsilon(\boldsymbol{k}) = \pm|f(\boldsymbol{k})|$, and the Dirac points, that we name $\boldsymbol{D}$ and $-\boldsymbol{D}$ are solutions of $f(\boldsymbol{D}) = 0$. Since $f(\boldsymbol{k}) = f^*(-\boldsymbol{k})$, the Dirac points, when they exist, necessarily come in by pairs [22]. The position $\boldsymbol{D}$ of the Dirac points can be anywhere in the BZ and move upon variation of the band parameters t_{mn}. Around the Dirac points $\pm\boldsymbol{D}$, the function $f(\boldsymbol{k})$ varies linearly. Writing $\boldsymbol{k} = \pm D + \boldsymbol{q}$, we find ($\hbar = 1$)

$$f(\pm\boldsymbol{D} + \boldsymbol{q}) = \boldsymbol{q}\cdot(\pm\boldsymbol{v}_1 - i\boldsymbol{v}_2) \tag{3}$$

where the velocities $\boldsymbol{v}_1$ and $\boldsymbol{v}_2$ are given by

$$\begin{aligned} \boldsymbol{v}_1 &= \sum_{mn} t_{mn}\boldsymbol{R}_{mn}\sin\boldsymbol{D}\cdot\boldsymbol{R}_{mn} \\ \boldsymbol{v}_2 &= \sum_{mn} t_{mn}\boldsymbol{R}_{mn}\cos\boldsymbol{D}\cdot\boldsymbol{R}_{mn}. \end{aligned} \tag{4}$$

Upon variation of the band parameters, the two Dirac points may approach each other and merge into a single point $\boldsymbol{D}_0$. This happens when $\boldsymbol{D} = -\boldsymbol{D}$ modulo a reciprocal lattice vector $\boldsymbol{G} = p\boldsymbol{a}_1^* + q\boldsymbol{a}_2^*$, where $\boldsymbol{a}_1^*$ and $\boldsymbol{a}_2^*$ span the reciprocal lattice. Therefore, the location of this merging point is simply $\boldsymbol{D}_0 = \boldsymbol{G}/2$. There are then four possible inequivalent points the coordinates of which are $\boldsymbol{D}_0 = (p\boldsymbol{a}_1^* + q\boldsymbol{a}_2^*)/2$, with $(p,q) = (0,0),(1,0),(0,1)$, and $(1,1)$. The condition $f(\boldsymbol{D}_0) = \sum_{mn}(-1)^{\beta_{mn}} t_{mn} = 0$, where $\beta_{mn} = pm + qn$, defines a manifold in the space of band parameters. As we discuss below, this manifold separates a semi-metallic phase with two Dirac cones and a band insulator.

In the vicinity of the $\boldsymbol{D}_0$ point, f is *purely imaginary* ($\boldsymbol{v}_1^0 = 0$), since $\sin(\boldsymbol{G}\cdot\boldsymbol{R}_{mn}/2) = 0$. Consequently, to lowest order, the linearized Hamiltonian reduces to $\mathcal{H} = \boldsymbol{q}\cdot\boldsymbol{v}_2^0\sigma^y$, where $\boldsymbol{v}_2^0 = \sum_{mn}(-1)^{\beta_{mn}} t_{mn}\boldsymbol{R}_{mn}$. We choose the local reference system such that $\boldsymbol{v}_2^0 \equiv c_y\,\hat{y}$ defines the y-direction [23]. In order to account for the dispersion in the local x-direction, we have to expand $f(\boldsymbol{D}_0 + \boldsymbol{q})$ to second order in $\boldsymbol{q}$:

$$f(\boldsymbol{D}_0 + \boldsymbol{q}) = -i\boldsymbol{q}\cdot\boldsymbol{v}_2^0 - \frac{1}{2}\sum_{mn}(-1)^{\beta_{mn}} t_{mn}(\boldsymbol{q}\cdot\boldsymbol{R}_{mn})^2. \tag{5}$$

Keeping the quadratic term in q_x, the new Hamiltonian may be written as

$$\mathcal{H}_0(\boldsymbol{q}) = \begin{pmatrix} 0 & \frac{q_x^2}{2m^*} - ic_y q_y \\ \frac{q_x^2}{2m^*} + ic_y q_y & 0 \end{pmatrix}, \tag{6}$$

where the effective mass m^* is defined by

$$\frac{1}{m^*} = \sum_{mn} (-1)^{\beta_{mn}+1} t_{mn} R_{mn,x}^2, \tag{7}$$

and where $R_{mn,x}$ is the component of $\boldsymbol{R}_{mn}$ along the *local* x-axis (perpendicular to $\boldsymbol{v}_2^0$). The terms of order q_y^2 and $q_x q_y$ are neglected at low energy [24]. The diagonalization of $\mathcal{H}_0(\boldsymbol{q})$ is straightforward and the energy spectrum

$$\epsilon = \pm \left[c_y^2 q_y^2 + \left(\frac{q_x^2}{2m^*} \right)^2 \right]^{1/2} \tag{8}$$

has a remarkable structure: it is linear in one direction and quadratic in the other. From the linear-quadratic hybrid spectrum which defines a velocity c_y and a mass m^*, one may identify a characteristic energy:

$$m^* c_y^2 = \frac{[\sum_{mn} (-1)^{\beta_{mn}} t_{mn} \boldsymbol{R}_{mn}]^2}{\sum_{mn} (-1)^{\beta_{mn}+1} t_{mn} R_{mn,x}^2}. \tag{9}$$

The merging of the Dirac points in D_0 marks the transition between a semi-metallic phase and an insulating phase. In this paper, we concentrate on the properties of the spectrum in the vicinity of the merging. The transition is driven by the parameter

$$\Delta = f(\boldsymbol{D}_0) = \sum_{mn} (-1)^{\beta_{mn}} t_{mn} \tag{10}$$

which changes its sign at the transition. In the vicinity of the transition, the Hamiltonian has the form

$$\mathcal{H}(\boldsymbol{q}) = \begin{pmatrix} 0 & \Delta + \frac{q_x^2}{2m^*} - i c_y q_y \\ \Delta + \frac{q_x^2}{2m^*} + i c_y q_y & 0 \end{pmatrix} \tag{11}$$

with the spectrum

$$\epsilon = \pm \sqrt{(\Delta + \frac{q_x^2}{2m^*})^2 + q_y^2 c_y^2} \tag{12}$$

where the wave vector $\boldsymbol{q}$ is now measured from the merging point and no longer from one of the Dirac points, i.e. $\boldsymbol{q} = 0$ denotes the merging point $\boldsymbol{D}_0$.

The Hamiltonian (11) has a remarkable structure and describes properly the vicinity of the topological transition, as shown in Figure 1. When $m^*\Delta$ is negative (we choose $m^* > 0$ without loss of generality), the spectrum exhibits the two Dirac cones and a saddle point in $\boldsymbol{D}_0$ (at half distance between the two Dirac points). Increasing Δ from negative to positive values, the saddle point evolves into the hybrid point at the transition ($\Delta = 0$) before a gap $2\Delta > 0$ opens.

In this paper, we study the spectral properties around the merging, in particular in the presence of a magnetic field. Moreover, we stress that this Hamiltonian has the general structure to describe the physics of Dirac points, even far from the transition, since it captures quite simply the coupling between the two valleys associated with the two Dirac points. In particular, we can relate the coupling between valleys to a double well potential problem. For this reason we name it a universal Hamiltonian.

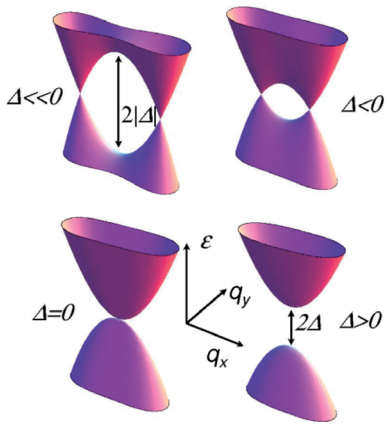

Fig. 1. (Color online) Evolution of the spectrum when the quantity Δ is varied and changes in sign at the topological transition (arbitrary units). The low-energy spectrum stays linear in the q_y direction.

3 Properties of the universal Hamiltonian

When Δ varies from negative to positive values, a topological transition from a semi-metallic phase with two Dirac cones to a band insulator with a gapped spectrum occurs. At the transition, the spectrum is hybrid, a reminiscence of the saddle point in the semi-metallic phase, see Figure 1.

When $\Delta < 0$, the spectrum exhibits two Dirac points the position of which along the x axis is given by $\pm q_D$ with

$$q_D = \sqrt{-2m^*\Delta} \tag{13}$$

and the linear spectrum around these Dirac points is characterized by the velocity c_x along the x direction:

$$c_x = \frac{q_D}{m^*} = \sqrt{\frac{-2\Delta}{m^*}}. \tag{14}$$

The two Dirac points are separated by a saddle point at position $q_S = 0$ whose energy is $\pm|\Delta|$. The mass m^* describes the curvature of the spectrum in the vicinity of this point along the x direction. When $\Delta < 0$ varies, the Dirac points move along the q_x axis.

The energy dispersion relation (12) is characterized by three parameters, the velocity c_y along the q_y direction, the mass m^* along the q_x direction and the gap Δ. Alternatively, it can be characterized by the distance $2q_D$ between the Dirac cones or the velocity c_x, or by any combination of two among the four parameters m^*, Δ, c_x, or q_D. In Table 1, we write explicitly all the combinations between these parameters. The universal Hamiltonian describes properly the vicinity of the Dirac points. Indeed, the spectrum can be linearized along the q_x direction, to recover an anisotropic Dirac equation in the vicinity of each point with a velocity c_x given by (14)

$$\mathcal{H} = \begin{pmatrix} 0 & \pm c_x \delta q_x - i c_y q_y \\ \pm c_x \delta q_x + i c_y q_y & 0 \end{pmatrix}$$

where $\delta q_x = q_x - q_D$.

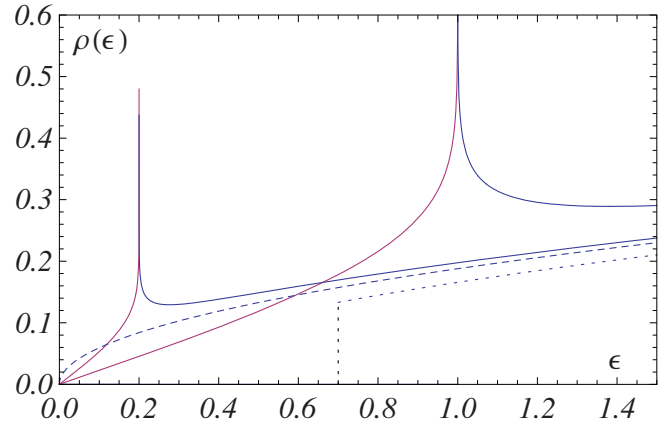

Fig. 2. (Color online) Evolution of the density of states on the metallic side of the transition ($\Delta < 0$), plotted for $\Delta = -1$ and $\Delta = -0.2$. For finite Δ, there is a linear dependence at low energy $\ll|\Delta|$, followed by a logarithmic singularity at $|\Delta|$. At the transition the density of states varies as $\sqrt{\epsilon}$ (dashed curve). Above the transition, there is a finite gap ($\Delta > 0$) and the density of states has a discontinuity (dotted curve for $\Delta = 0.7$). Here we have fixed $m^* = c_y = 1$.

Table 1. In addition to the velocity c_y, the universal Hamiltonian is described by two independent parameters (left column) from which two other parameters may be deduced.

q_D, m^*	$c_x = q_D/m^*$	$\Delta = -q_D^2/2m^*$
q_D, c_x	$m^* = q_D/c_x$	$\Delta = -c_x q_D/2$
m^*, c_x	$q_D = m^* c_x$	$\Delta = -m^* c_x^2/2$
m^*, Δ	$c_x = \sqrt{-2\Delta/m^*}$	$q_D = \sqrt{-2m^*\Delta}$
c_x, Δ	$q_D = -2\Delta/c_x$	$m^* = -2\Delta/c_x^2$
q_D, Δ	$m^* = -q_D^2/2\Delta$	$c_x = -2\Delta/q_D$

In Section 4, we discuss which combination of parameters should be taken in order to properly describe the low energy physics of the $t - t'$ model of the honeycomb lattice.

3.1 Density of states

We have calculated the density of states for the energy dispersion (12). We find, below the transition ($\Delta < 0$),

$$\begin{aligned} \epsilon < |\Delta| \quad &\rightarrow \quad \rho(\epsilon) = \frac{\sqrt{2m^*}}{\pi^2 c_y} \frac{\epsilon}{\sqrt{\epsilon - \Delta}} K\left(\sqrt{\frac{2\epsilon}{\epsilon - \Delta}}\right) \\ \epsilon > |\Delta| \quad &\rightarrow \quad \rho(\epsilon) = \frac{\sqrt{2m^*}}{\pi^2 c_y} \sqrt{\frac{\epsilon}{2}} K\left(\sqrt{\frac{\epsilon - \Delta}{2\epsilon}}\right) \end{aligned} \tag{15}$$

where $K(x)$ is the complete elliptic integral of the first kind [26]. In the low energy limit, one recovers the familiar linear energy dependence $\rho(\epsilon) = \frac{1}{\pi c_x c_y}\epsilon$. The density of states exhibits a logarithmic divergence at $\epsilon = |\Delta|$, due to the saddle point. It is plotted in Figure 2 for a fixed mass m^*, and upon variation of the parameter Δ. When approaching the transition, the weight of the logarithmic singularity vanishes and, at the transition, one recovers the density of states found in reference [4], given by

$$\rho(\epsilon) = C \frac{\sqrt{m^*}}{c_y} \epsilon^{1/2} \tag{16}$$

where $C = \frac{1}{\pi^2} K(1/\sqrt{2}) = \Gamma(1/4)^2/(4\pi^{5/2}) \simeq 0.188$.

Above the transition, there is a finite gap $\Delta > 0$ and the density of states has a jump at $\epsilon = \Delta$:

$$\begin{aligned} \epsilon < \Delta \quad &\rightarrow \quad \rho(\epsilon) = 0 \\ \epsilon > \Delta \quad &\rightarrow \quad \rho(\epsilon) = \frac{\sqrt{2m^*}}{\pi^2 c_y} \sqrt{\frac{\epsilon}{2}} K\left(\sqrt{\frac{\epsilon - \Delta}{2\epsilon}}\right). \end{aligned} \tag{17}$$

3.2 Specific heat

Since the spectrum has the electron-hole symmetry $\rho(\epsilon) = \rho(-\epsilon)$, the chemical potential is temperature independent and fixed at $\mu = 0$ for the undoped system. Therefore the specific heat has the general form ($k_B = 1$)

$$C(T) = \frac{\beta^2}{2} \int_0^\infty \frac{\epsilon^2 \rho(\epsilon) d\epsilon}{\cosh^2 \frac{\beta\epsilon}{2}} \tag{18}$$

where $\beta = 1/T$. Using the expression (15) of the density of states, we obtain, on the metallic side ($\Delta < 0$)

$$C(T) = 4 \frac{\sqrt{2m^*}}{\pi^2 c_y} T^{3/2} f\left(\frac{T}{|\Delta|}\right) \tag{19}$$

where the function $f(T/|\Delta|)$ is given by

$$\begin{aligned} f(t) = &\int_0^{1/2t} \frac{2\sqrt{t}\, x^3}{\sqrt{2xt+1}\cosh^2 x} K\left(\sqrt{\frac{4x}{2xt+1}}\right) dx \\ &+ \int_{1/2t}^\infty \frac{x^{5/2}}{\cosh^2 x} K\left(\sqrt{\frac{2xt+1}{4x}}\right) dx. \end{aligned} \tag{20}$$

It is plotted in Figure 3 (top) and it has the following limits

$$\begin{aligned} t \to 0 \qquad & f(t) \to \frac{9\pi}{8}\zeta(3)\sqrt{t} \simeq 4.248\sqrt{t} \\ t \to \infty \qquad & f(t) \to \frac{15}{256}(\sqrt{8}-1)\Gamma(1/4)^2\zeta(5/2) \simeq 1.889 \end{aligned}$$

so that the low T specific heat interpolates from a T^2 behavior far from the transition to a $T^{3/2}$ behavior at the transition. Similarly, above the transition, in the insulating phase ($\Delta > 0$), we find, using (17):

$$C(T) = 4 \frac{\sqrt{2m^*}}{\pi^2 c_y} T^{3/2} g\left(\frac{T}{\Delta}\right) \tag{21}$$

where the function $g(T/\Delta)$ is given by

$$g(t) = \int_{1/2t}^\infty \frac{x^{5/2}}{\cosh^2 x} K\left(\sqrt{\frac{2xt-1}{4x}}\right) dx. \tag{22}$$

The function $g(t)$, plotted on Figure 3 (bottom), varies exponentially at small t, so that the low T specific heat interpolates from the $T^{3/2}$ behavior at the transition to an activated behavior.

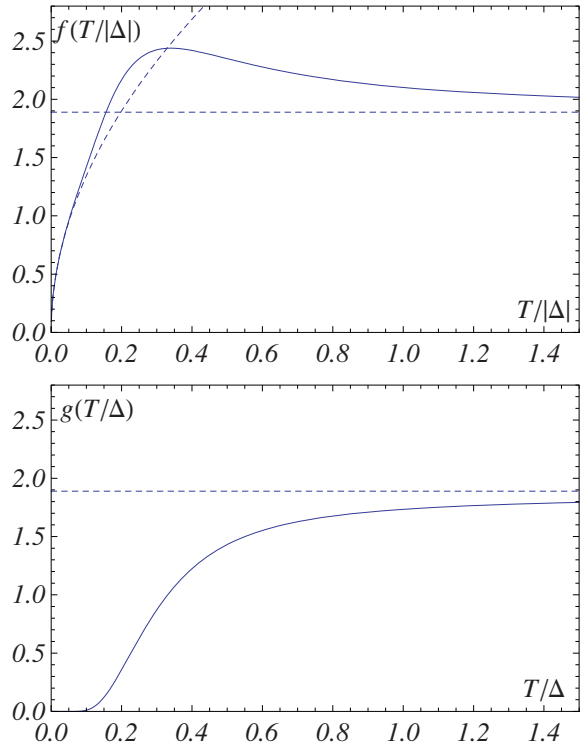

Fig. 3. (Color online) Top figure: function $f(t = T/|\Delta|)$ entering the expression of the specific heat (19), in the metallic phase ($\Delta < 0$). Bottom figure: function $g(t = T/\Delta)$ entering the expression of the specific heat (21), in the insulating phase ($\Delta > 0$). The dashed curves show the asymptotic behaviors.

3.3 Landau quantization

We now calculate the spectrum of the universal Hamiltonian in the presence of a magnetic field B. In the Landau gauge $\boldsymbol{A} = (0, Bx, 0)$, the substitution $q_x \to q_x - eBy$ leads to the new Hamiltonian

$$\mathcal{H} = \begin{pmatrix} 0 & \Delta + \frac{1}{2}m^*\omega_c^2\tilde{y}^2 - ic_y q_y \\ \Delta + \frac{1}{2}m^*\omega_c^2\tilde{y}^2 - ic_y q_y & 0 \end{pmatrix}$$

where, as usual, $\tilde{y} = y - q_x/eB$. The spectrum in the bulk does not depend on the shift q_x/eB. We introduce the dimensionless variables $Y = \tilde{y}/\alpha$ and $P = \alpha q_y$, so that $[X, P] = i$. We obtain the effective magnetic length for this problem $\alpha = \left(\frac{2c_y}{m^*\omega_c^2}\right)^{1/3} = (2m^* c_y \ell_B^4)^{1/3}$, where $\ell_B = 1/\sqrt{eB}$ is the usual magnetic length. The Hamiltonian is rewritten as

$$\mathcal{H} = \left(\frac{m^*\omega_c^2 c_y^2}{2}\right)^{1/3} \begin{pmatrix} 0 & \delta + Y^2 - iP \\ \delta + Y^2 + iP & 0 \end{pmatrix}. \quad (23)$$

Squaring this Hamiltonian, we have to solve the effective Schrödinger equation

$$\epsilon_n^2 \psi^{A,B} = \left(\frac{m^*\omega_c^2 c_y^2}{2}\right)^{2/3} \left(P^2 + (\delta + Y^2)^2 - is[P, Y^2]\right) \psi^{A,B}$$

where $s = \pm 1$ corresponds to the two sites A and B. We have introduced the dimensionless gap

$$\delta = \frac{\Delta}{\left(\frac{m^*\omega_c^2 c_y^2}{2}\right)^{1/3}} \propto \frac{\Delta}{B^{2/3}}. \quad (24)$$

We now have to diagonalize the effective Hamiltonian $\mathcal{H}_{\mathit{eff}}$:

$$\mathcal{H}_{\mathit{eff}} = P^2 + (\delta + Y^2)^2 - 2sY, \quad (25)$$

and the eigenvalues ϵ_n of the original problem (23) are related to the eigenvalues E_n of this effective Hamiltonian (25) by

$$\epsilon_n = \pm \left(\frac{m^*\omega_c^2 c_y^2}{2}\right)^{1/3} \sqrt{E_n(\delta)} = \pm \frac{\Delta}{\delta} \sqrt{E_n(\delta)} \quad (26)$$

where δ is given by (24). We thus obtain the general scaling behavior of the Landau levels:

$$\epsilon_n \propto B^{2/3} f_n(\Delta/B^{2/3}). \quad (27)$$

When varying δ, this Hamiltonian has the remarkable property to describe continuously the Landau level spectrum from the $\epsilon_n \propto \sqrt{nB}$ dependence with double degeneracy for well separated Dirac cones to the $\epsilon_n \propto (n+1/2)B$ usual dependence for a massive particle. The physics behind is that for negative δ, the problem is similar to the one of a particle in a double well potential. In the limit of large negative δ, that is far from the transition or in a weak magnetic field, the potential has two well separated valleys which are almost uncoupled. This corresponds to the situation of two independent valleys. Note that in this limit the energy shift between the two valleys is $2\sqrt{\delta}$. When δ diminishes, we progressively increase the coupling between valleys. The degeneracy of Landau levels is progressively lifted, as shown in Figure 4.

We have solved numerically the Hamiltonian $\mathcal{H}_{\mathit{eff}}$. Eigenvalues are given in Figure 5 as functions of δ. We now comment our results and the different limits.

- If $\delta < 0$, we have to solve the problem of a double well potential (Fig. 4a) (and independent wells in the limit $|\delta| \gg 1$). The potential has two minima for $Y_0 = \pm\sqrt{|\delta|}$. In real space, the distance $2Y_0$ corresponds to the distance $2y_0 = 2\alpha Y_0 = 2q_D\ell_B^2$, where ℓ_B is the magnetic length. An expansion around these minima $Y = \pm\sqrt{\delta} + x$ gives the effective Hamiltonian:

$$\mathcal{H}_{\mathit{eff}} = P^2 + 4|\delta|x^2 \mp 2s\sqrt{|\delta|}.$$

Introducing the new variables $p' = P/(\sqrt{2}|\delta|^{1/4})$ and $x' = x\sqrt{2}|\delta|^{1/4}$, this Hamiltonian reduces to

$$\mathcal{H}_{\mathit{eff}} = 2\sqrt{|\delta|}(p'^2 + x'^2 \pm 1)$$

with eigenvalues

$$E_n = 4n\sqrt{|\delta|}. \quad (28)$$

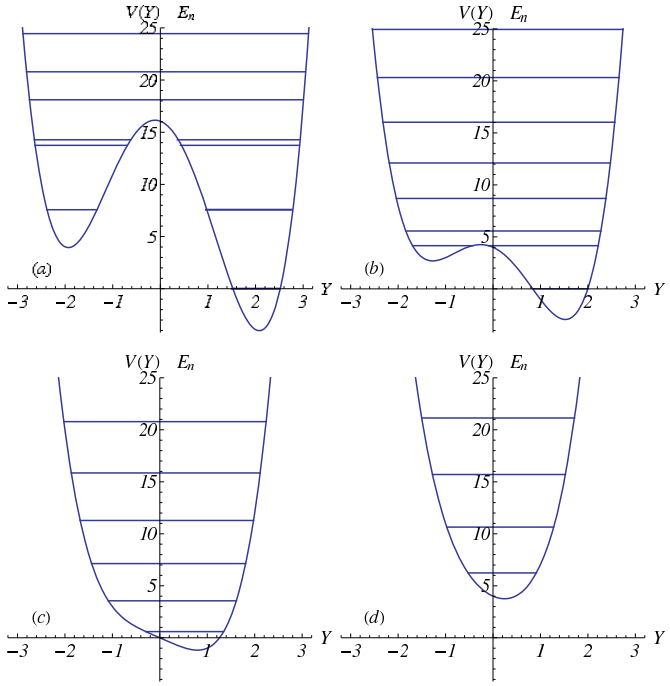

Fig. 4. (Color online) Potential profile and energy levels E_n of the Hamiltonian $\mathcal{H}_{eff} = P^2 + (\delta + Y^2)^2 - 2Y$, for $\delta = -4$, $-2, 0, 2$.

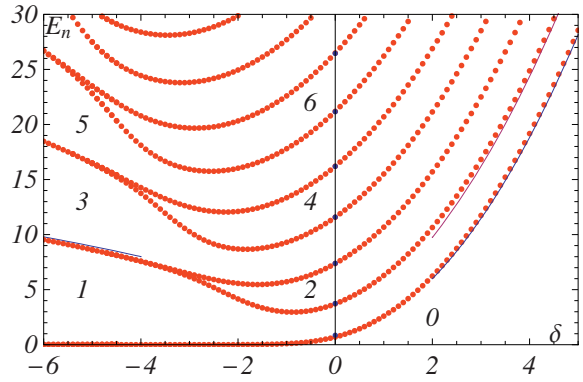

Fig. 5. (Color online) Energy levels $E_n(\delta)$ of the Hamiltonian $\mathcal{H}_{eff} = P^2 + (\delta + Y^2)^2 - 2Y$. We have plotted asymptotic analytical behaviors, $E_n = 4n\sqrt{-\delta}$ for large negative δ and $E_n = \delta^2 + 4(n + 1/2)\sqrt{\delta}$ for large positive δ.

Each level $n \neq 0$ is doubly degenerate, due to the twofold structure of the potential well. We deduce that

$$\epsilon_n^2 = 4\frac{\Delta^2}{|\delta|^{3/2}}n$$

which can be written in the usual form, introducing $c_x = \sqrt{-2\Delta/m^*}$

$$\epsilon_n = \pm\sqrt{2nec^2B}$$

with the velocity c defined as

$$c = \sqrt{c_x c_y}.$$

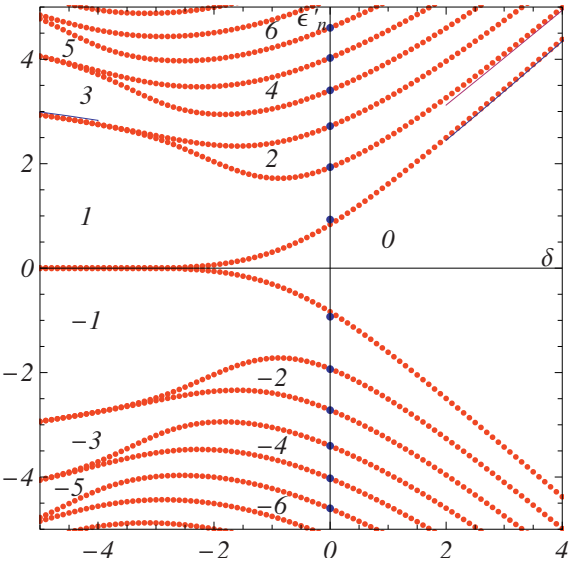

Fig. 6. (Color online) Energy levels $\epsilon'_n(\delta) = \epsilon_n(\delta)/(m^*\omega_c^2 c_y^2/2)^{1/3}$ as a function of the dimensionless gap δ. The blue dots on the $\delta = 0$ axis indicate the semiclassical levels of the quartic Hamiltonian.

Each energy level ϵ_n is doubly degenerate. We recover the well-known result for two independent Dirac valleys, generalized here to the anisotropic case.

- When $|\delta|$ diminishes, the potential barrier between the two valleys decreases and tunneling between the valleys removes the twofold degeneracy of each level (Fig. 4b). We can estimate the shift of the levels due to a finite Δ. The shift is proportional to the probability to tunnel between the two valleys. It scales as $\delta E_n \propto e^{-\sqrt{V-E_n}d}$ where the potential height V is proportional to $|\delta|^2$ and the distance between valleys d is proportional to $\sqrt{|\delta|}$. As a result, the level degeneracy is lifted as [27]

$$e^{-\#|\delta|^{3/2}} \sim e^{-\#|\Delta|^{3/2}/B}. \tag{29}$$

- At the transition point, $\delta = 0$, the energy levels are those of a modified quartic oscillator with a potential $V(Y) = Y^4 - 2Y$ and they have been obtained in reference [4] and are well approximated by:

$$E_n = C(n + 1/2)^{4/3} \tag{30}$$

with $C = \pi^2[3\sqrt{2}/\Gamma(1/4)^2]^{4/3} \simeq 2.185$. From equation (26), we deduce the following dependence of the Landau levels

$$\epsilon_n = \pm A(m^* c_y^2)^{1/3}[(n + 1/2)\omega_c]^{2/3} \tag{31}$$

with $A = \sqrt{C/2^{2/3}} \simeq 1.173$. In reference [4], we have studied in detail the effect of the linear term in the potential $V(Y)$, which only slightly changes the above result. We have attributed the phase term 1/2 to the annihilation of the Berry phases attached to each Dirac point at their merging. This is also briefly discussed in the next subsection of this paper.

- For large $\delta > 0$, the Hamiltonian can be expanded and transformed into a quadratic Hamiltonian

$$\mathcal{H}_{\mathit{eff}} = P^2+\delta^2+2\delta Y^2-2Y \simeq P^2+\delta^2+2\delta(Y-1/(2\delta))^2 \tag{32}$$

so that the spectrum is again the one of an harmonic oscillator

$$E_n = \delta^2 + 2\sqrt{2}(n'+1/2)\sqrt{\delta} \tag{33}$$

and we recover a usual Landau spectrum in the gapped phase:

$$\epsilon_n = \pm\left(\Delta + \sqrt{\frac{m^*c^2}{\Delta}}(n+1/2)\omega_c\right). \tag{34}$$

3.4 Berry's phase

We now briefly turn to the structure of the wave functions, solutions of the universal Hamiltonian (11). They are of the form

$$\psi(\boldsymbol{r}) = \frac{1}{\sqrt{2}}\begin{pmatrix}1\\ e^{i\theta_{\boldsymbol{q}}}\end{pmatrix} e^{i\boldsymbol{q}\cdot\boldsymbol{r}} \tag{35}$$

where the two components refer to the two sublattices A and B. The phase $\theta_{\boldsymbol{q}}$ is given by

$$\tan\theta_{\boldsymbol{q}} = \frac{c_y q_y}{\Delta + \frac{q_x^2}{2m^*}}. \tag{36}$$

Note that the two valleys, centered on $q_x = \pm q_D = \pm\sqrt{-2m^*\Delta}$ and $q_y = 0$, are described by the *same* wave function. The $\boldsymbol{q}$ dependence of $\theta_{\boldsymbol{q}}$ is shown in Figure 7 and exhibits a vortex structure around the two Dirac points. Each point is characterized by a Berry phase $\frac{1}{2}\oint \nabla\theta_q \cdot d\boldsymbol{q} = \pm\pi$. Figure 7 shows the annihilation of the two Berry phases at the topological transition. This is the reason why the Landau levels acquire a $n+1/2$ dependence in the vicinity and above the topological transition (see next section) [28].

3.5 Semiclassical quantization and integrated density of states

It is instructive to derive the energy levels from semiclassical Bohr-Sommerfeld quantization: along one period of the motion, the action must be quantized [25]. This condition can be written as

$$\mathcal{S}(\epsilon) = 2\pi(n+\gamma)eB, \tag{37}$$

where $\mathcal{S}(\epsilon)$ is the area of a cyclotron orbit of energy ϵ is reciprocal space. It is simply $\mathcal{S}(\epsilon) = 4\pi^2 N(\epsilon)$ where $N(\epsilon)$ is the integrated density of states which can be obtained from expressions (15). The phase mismatch γ is the sum of two contributions $\gamma = \gamma_M + \gamma_B$ where $\gamma_M = 1/2$ is the Maslov contribution and γ_B results from the Berry phase. We obtain, for $0 < \epsilon < -\Delta$:

$$\mathcal{S}(\epsilon) = \frac{4}{3}\frac{\sqrt{2m^*(\epsilon-\Delta)}}{c_y} \times\left[(\epsilon+\Delta)K\left(\sqrt{\frac{2\epsilon}{\epsilon-\Delta}}\right) - \Delta E\left(\sqrt{\frac{2\epsilon}{\epsilon-\Delta}}\right)\right] \tag{38}$$

where $K(x)$ and $E(x)$ are respectively complete elliptic integrals of the first and of the second kind [26]. This quantity represents the area enclosed by *each* of the two degenerate equal energy lines encircling one Dirac point (Fig. 8). The phase mismatch cancels here due to a finite Berry phase $\gamma_B = \pm 1/2$ [28], so that the quantization condition is $\mathcal{S}(\epsilon) = 2\pi neB$.

Similarly, for $\epsilon > -\Delta$:

$$\mathcal{S}(\epsilon) = \frac{8}{3}\frac{\sqrt{m^*\epsilon}}{c_y} \times\left[(\epsilon+\Delta)K\left(\sqrt{\frac{\epsilon-\Delta}{2\epsilon}}\right) - 2\Delta E\left(\sqrt{\frac{\epsilon-\Delta}{2\epsilon}}\right)\right] \tag{39}$$

and the quantization condition is now $\mathcal{S}(\epsilon) = 2\pi(n'+1/2)eB$. The contribution γ_B is cancelled since the semiclassical trajectories enclose the two Dirac points and the Berry phase is 0.

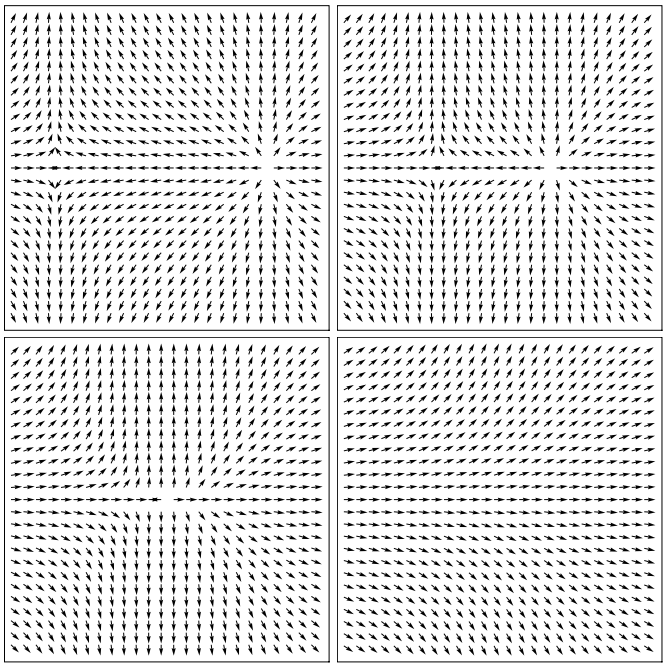

Fig. 7. Relative phase $\theta_{\boldsymbol{q}}$ of the two-component wave function. The four plots correspond respectively from left to right and then from top to bottom: $\Delta = -1, -.3, 0, 1$ ($m^* = c_y = 1$). In the insulating phase, two opposite Berry phases are attached to the two Dirac points. The Berry phases annihilate at the transition point.

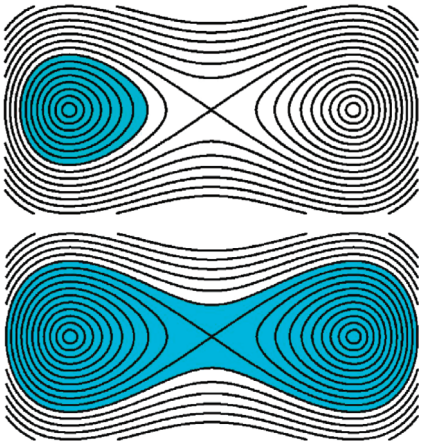

Fig. 8. (Color online) Semiclassical quantization of area. When $\epsilon < -\Delta$, the quantization of energy levels results from the quantization of orbits in each valley $S(\epsilon) = 2\pi neB$ and the spectrum has the double valley degeneracy. When $\epsilon > -\Delta$, above the saddle point, the quantization implies larger orbits which encircle the two Dirac valleys, and it reads $S(\epsilon) = 2\pi(n' + 1/2)eB$.

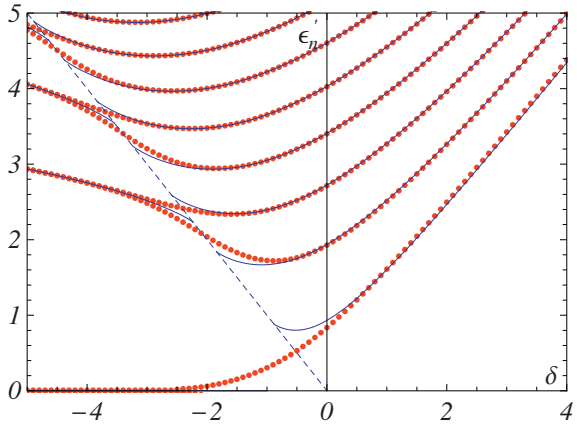

Fig. 9. (Color online) Positive exact energy levels $\epsilon_n'(\delta) = \epsilon_n(\delta)/(m^*\omega_c^2 c_y^2/2)^{1/3}$ (dots) compared with the result of semiclassical quantization (lines). The dashed line $\epsilon_n' = -\delta$ corresponds to $\epsilon_n = -\Delta$, that is to the energy of the saddle point. The discontinuity is due to the doubling of the area $S(\epsilon)$ and to the cancellation of the Berry phase when energy crosses the saddle point.

Figure 9 compares the real spectrum with the above semiclassical quantization. The approximation works very well except in the vicinity of the transition line $\epsilon_n = -\Delta$ which corresponds to the energy of the saddle point. It is worth stressing that the semiclassical approximation describes perfectly well the vicinity of the topological transition (near $\delta = 0$ axis in Fig. 9). The energy levels are given by the dimensionless equations

$$\epsilon < -\Delta \quad \rightarrow \quad F_-\left(\frac{\epsilon}{\Delta}\right) = \frac{3\pi}{2}\frac{n}{|\delta|^{3/2}} \tag{40}$$

$$\epsilon > -\Delta \quad \rightarrow \quad F_+\left(\frac{\epsilon}{\Delta}\right) = \frac{3\pi}{2\sqrt{2}}\frac{n'+1/2}{|\delta|^{3/2}} \tag{41}$$

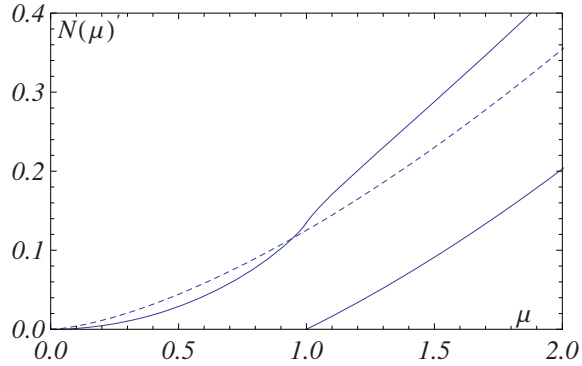

Fig. 10. (Color online) Energy dependence of the integrated density of states. We have fixed $m^* = c_y = 1$. The upper continuous curve corresponds to the metallic phase $\Delta = -1$, it has a singularity at $\mu = -\Delta$, and varies as μ^2 for $\mu \ll -\Delta$. Above the transition ($\Delta = +1$, lower continuous line), it is zero in the gap region and then varies linearly. At the transition (dashed curve), it varies as $\mu^{3/2}$.

with

$$F_-(r) = \sqrt{1-r}\left[E\left(\sqrt{\frac{2r}{r-1}}\right) - (r+1)K\left(\sqrt{\frac{2r}{r-1}}\right)\right] \tag{42}$$

$$F_+(r) = \sqrt{|r|}\left|2E\left(\sqrt{\frac{r-1}{2r}}\right) - (r+1)K\left(\sqrt{\frac{r-1}{2r}}\right)\right|. \tag{43}$$

3.6 Density profile measurement

There have been several suggestions for the realization of Dirac fermions and their merging in an anisotropic honeycomb optical lattice [6,13–16]. In this case, the method used to probe the dispersion relation is a density profile measurement which directly gives access to the density of particles. One then has to measure this quantity as a function of the chemical potential μ. At zero temperature, this quantity is nothing but the integrated density of states calculated in the above subsection $N(\mu) = \int_0^\mu \rho(\epsilon)d\epsilon$. It can be reconstructed through a time of flight experiment, as explained in reference [13]. In Figure 10, we plot the integrated density of states for the universal Hamiltonian, following the lines of reference [13].

4 Application to graphene and the honeycomb lattice

We now propose that the universal Hamiltonian constitutes an excellent description of the low energy physics of the $t-t'$ model including the two valleys. First we briefly recall the electronic structure of graphene, and assume more generally that one of the three hopping parameters t' between nearest neighbors may be different from the two others t, as shown in Figure 11.

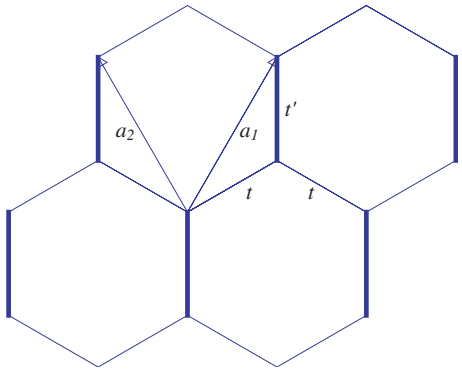

Fig. 11. (Color online) Honeycomb lattice with hopping integrals t and t', and elementary vectors $\boldsymbol{a}_1$ and $\boldsymbol{a}_2$ discussed in the text.

The tight-binding Hamiltonian couples sites of different sublattices named A and B. The eigenvectors are Bloch waves of the form

$$|\boldsymbol{k}\rangle = \frac{1}{\sqrt{N}} \sum_j \left(c_{\boldsymbol{k}}^A |\boldsymbol{R}_j^A\rangle + c_{\boldsymbol{k}}^B |\boldsymbol{R}_j^B\rangle \right) e^{i\boldsymbol{k}\cdot\boldsymbol{R}_j} \qquad (44)$$

where $|\boldsymbol{R}_j^A\rangle, |\boldsymbol{R}_j^B\rangle$ are atomic states. The sum runs over vectors of the Bravais lattice. The Hamiltonian has the form (1), with

$$f(\boldsymbol{k}) = t' + te^{i\boldsymbol{k}\cdot\boldsymbol{a}_1} + te^{i\boldsymbol{k}\cdot\boldsymbol{a}_2} \qquad (45)$$

where $\boldsymbol{a}_1 = a(\frac{\sqrt{3}}{2}, \frac{3}{2})$, $\boldsymbol{a}_2 = a(-\frac{\sqrt{3}}{2}, \frac{3}{2})$ are elementary vectors of the Bravais lattice, a is the interatomic distance, and t, t' are shown in Figure 11. In Cartesian units

$$f(\boldsymbol{k}) = t' + 2t\cos\frac{\sqrt{3}}{2}k_x a \; e^{i\frac{3}{2}k_y a}. \qquad (46)$$

The energy, given by $\epsilon(\boldsymbol{k}) = \pm|f(\boldsymbol{k})|$, is shown in Figure 12 in the form of equal energy lines.

The evolution of the low energy spectrum when t' varies is plotted in Figure 13. It is obviously well described by our universal Hamiltonian (compare with Fig. 1). In the following, we carefully map the two models on each other.

When $t' = t$, the energy vanishes at the two points $\boldsymbol{D}$ and $\boldsymbol{D}'$ located at the corners $\boldsymbol{K}$ and $\boldsymbol{K}'$ of the Brillouin zone $\boldsymbol{K} = 2\boldsymbol{a}_1^*/3 + \boldsymbol{a}_2^*/3$, $\boldsymbol{K}' = \boldsymbol{a}_1^*/3 + 2\boldsymbol{a}_2^*/3$, where $\boldsymbol{a}_1^*$ and $\boldsymbol{a}_2^*$ are reciprocal lattice vectors) or, in Cartesian units

$$\boldsymbol{D} = \boldsymbol{K} = \left(\frac{2\pi}{3\sqrt{3}a}, \frac{2\pi}{3a}\right), \quad \boldsymbol{D}' = \boldsymbol{K}' = \left(\frac{-2\pi}{3\sqrt{3}a}, \frac{2\pi}{3a}\right). \qquad (47)$$

As t' increases, the two points $\boldsymbol{D}$ and $\boldsymbol{D}'$ approach each other. Their position is given by

$$\boldsymbol{D}\ /\boldsymbol{D}' = \left(\pm\frac{2}{3a}\arctan\sqrt{\frac{4t^2}{t'^2} - 1}, \frac{2\pi}{3a}\right). \qquad (48)$$

They merge into the single point $\boldsymbol{D}_0 = (\boldsymbol{a}_1^* + \boldsymbol{a}_2^*)/2 = (0, \frac{2\pi}{3a})$ when $t' = 2t$ (for $t' > 2t$, a gap opens between the two subbands). ($a = 1$ for shorter notations)

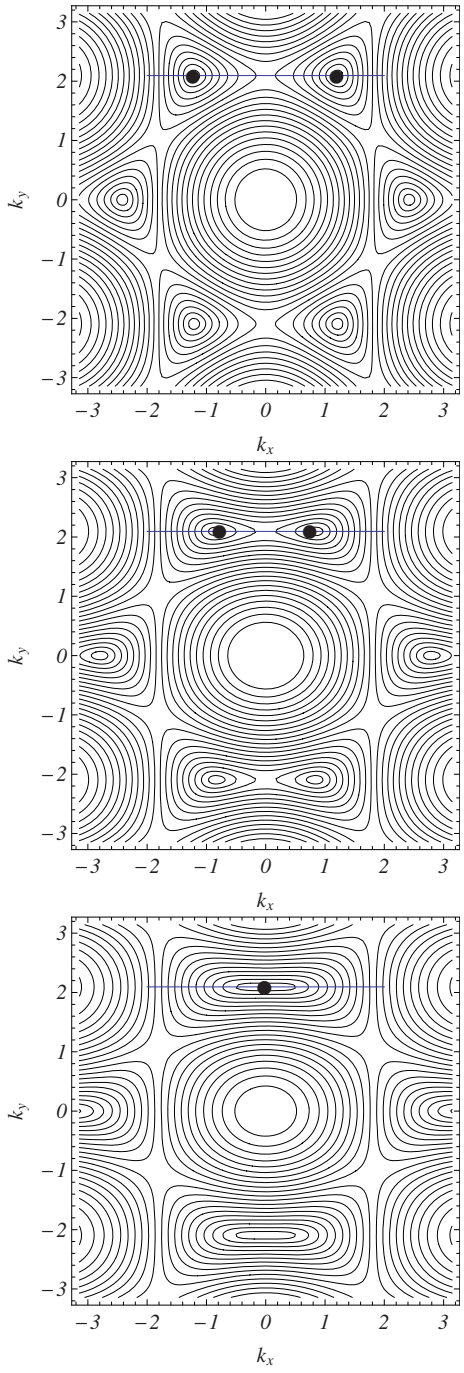

Fig. 12. Isoenergy lines for the $t-t'$ model with $t'/t = 1, 1.5, 2$, from top to bottom.

We now concentrate on the vicinity of the $\boldsymbol{KK'}$ axis, that is the line $k_y = 2\pi/3$. An expansion near this line, gives ($k_y = 2\pi/3 + q_y, k_x = q_x$):

$$f(\boldsymbol{q}) = t' - 2t\cos\frac{\sqrt{3}}{2}q_x - 3itq_y\cos\frac{\sqrt{3}}{2}q_x. \qquad (49)$$

We now wish to describe this Hamiltonian by the universal Hamiltonian (11), that is

$$f(\boldsymbol{q}) = \Delta - ic_y q_y + \frac{q_x^2}{2m^*} \qquad (50)$$

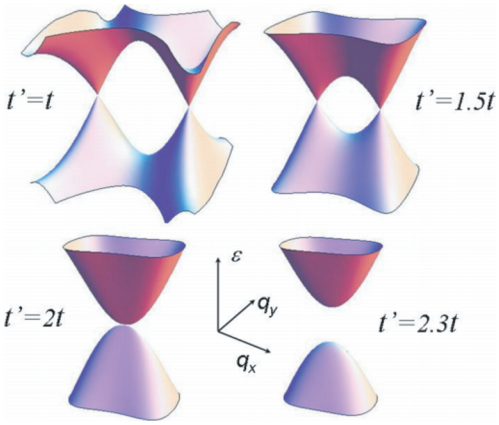

Fig. 13. (Color online) Evolution of the low energy spectrum when t' approaches t, in the $t-t'$ model of the honeycomb lattice. This evolution is very well described by the universal Hamiltonian (see Fig. 1).

for which we recall that fixing Δ and m^* imposes the position $\pm q_D$ of the Dirac points and the velocity c_x (see Tab. 1). We are now facing several possible choices to properly introduce the effective Hamiltonian. We may choose to fix the mass m^* and the parameter Δ by comparing the expansion of (49) near $q_x = 0$:

$$f(\boldsymbol{q}) = t' - 2t + \frac{3}{4}tq_x^2 - 3itq_y \tag{51}$$

with (50). This leads to

$$\Delta = t' - 2t, \quad m^* = \frac{2}{3t}, \quad c_y = 3t \tag{52}$$

and q_D and c_x are obtained from Table 1 and are plotted in Figure 14. This is not a good choice because, if it properly describes the spectrum near $q_x = 0$, it does not correctly describe the vicinity of the Dirac points $\pm q_D$.

We may also choose to fix Δ and the distance $2q_D$ between the Dirac points and the velocity c_y around the Dirac points

$$\Delta = t' - 2t, \quad q_D = \frac{2}{\sqrt{3}} \arctan \sqrt{\frac{4t^2}{t'^2} - 1}, \quad c_y = \frac{3}{2}t' \tag{53}$$

so that the mass and the velocity c_x are deduced from Table 1 and are plotted in Figure 14. With this choice the velocity near the Dirac points is not correct, so that the low energy spectrum when the Dirac points are far apart cannot be reproduced.

Among other possibilities we finally choose to fix Δ and the velocities c_x and c_y. Comparing (50) with the linear expansion of (49) near the Dirac points

$$f(\boldsymbol{q}) = \frac{3}{2}it'q_y \pm \sqrt{3(t^2 - t'^2/4)}q_x$$

where the $\pm$ sign denotes the vicinity of the two points $\boldsymbol{D}$ and $\boldsymbol{D'}$, we are led to choose the combination of parameters:

$$\Delta = t' - 2t, \quad c_x = \sqrt{3}\sqrt{t^2 - t'^2/4}, \quad c_y = \frac{3t'}{2} \tag{54}$$

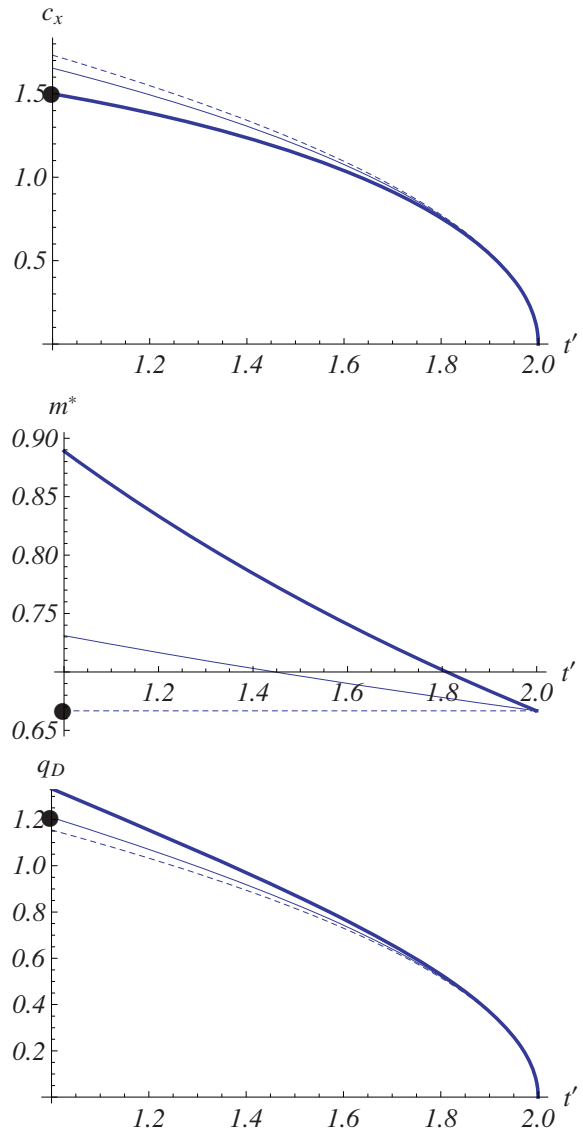

Fig. 14. (Color online) Plots of the dependence of the quantities c_x, m^* and q_D as a function of t' (here $t = 1$). The three lines correspond to three possible fits, where the mass m^* is fixed (dashed lines), the position q_D of the Dirac points is fixed (thin lines), or the velocity c_x is fixed, as chosen in the text (thick lines). The dot indicates the correct variation in the t, t' model.

from which we deduce the effective mass

$$m^* = \frac{-2\Delta}{c_x^2} = \frac{8}{3(2t + t')}. \tag{55}$$

This last choice of parameter is the best one since it properly describes the low energy spectrum with the correct velocities (see Fig. 14). Note that the low energy spectrum is not monotonic when t' increases since the product $c^2 = c_x c_y$ first increases and then decreases with t' (Fig. 15).

Using these parameters, we can now apply the results of the universal Hamiltonian (Figs. 5, 6) to the specific $t-t'$ model. We first introduce the reduced flux $f = \phi/\phi_0$, where ϕ is the flux through one elementary cell of the

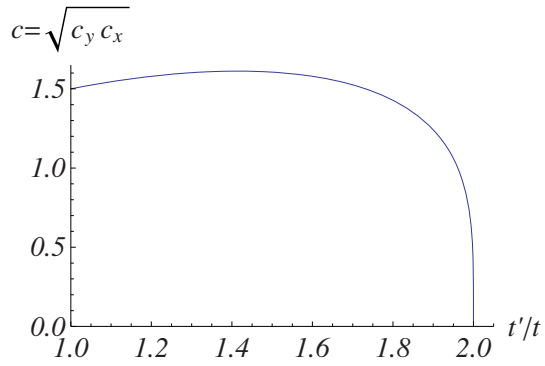

Fig. 15. (Color online) Non-monotonic behavior of the velocity $c = \sqrt{c_x c_y} = \frac{3^{3/4}}{2}\sqrt{t'}(4t^2 - t'^2)^{1/4}$ as a function of t'/t. The velocity is plotted in units of t ($\hbar = a = 1$).

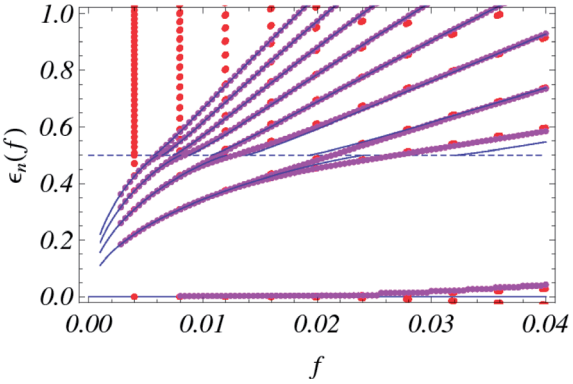

Fig. 16. (Color online) Red dots: flux dependence of the energy levels of the tight binding model on the honeycomb lattice with $t' = 1.5t$ [20]. Violet dots: energy levels calculated from the solutions of the 1D Schrödinger equation with a double well potential $V(Y) = (\delta - Y^2)^2 - 2Y$. Full continuous lines: result of the semiclassical quantization rule. Dashed line: line $\epsilon = -\Delta = 2t - t'$.

honeycomb lattice, and $\phi_0 = h/e = 2\pi/e$ is the flux quantum. We have $f = Ba^2 3\sqrt{3}/(2\phi_0) = \frac{3\sqrt{3}}{4\pi}eB$, since we have chosen $a = 1$, $\hbar = 1$. From our study of the universal Hamiltonian, the energy levels are given by (26)

$$\epsilon_n(f) = \pm\frac{t' - 2t}{\delta}\sqrt{E_n(\delta)} \tag{56}$$

where the function $E_n(\delta)$ has been studied in Section 3.3 (Fig. 5) and the parameter δ is deduced from the parameters (54, 55). We have

$$\delta = \left(\frac{2}{\pi}\right)^{2/3}\frac{t' - 2t}{[(2t + t')t'^2]^{1/3}}\frac{1}{f^{2/3}}. \tag{57}$$

In particular, in low field:

$$\epsilon_n = \pm\sqrt{2nec_x c_y B} = \sqrt{2\pi nt'(4t^2 - t'^2)^{1/2}}\sqrt{f}. \tag{58}$$

Figure 16 represents the energy levels for the honeycomb lattice with $t' = 1.5t$. The spectrum is represented as a function of the reduced flux f. In low field, the levels have a $\sqrt{nf}$ behavior. Then the degeneracy of the levels is lifted as predicted in equation (29), that is $\Delta\epsilon \propto e^{-\#(2t-t')^{3/2}/f}$. The overall spectrum is quite well described by the semiclassical quantization rule explicited in Section 3.5.

5 Summary

We have shown that the motion and merging of Dirac points in a two-dimensional crystal can be fully described by a simple 2×2 Hamiltonian with a linear dispersion relation in one direction, a massive term in the other direction, and a gap term Δ. By varying Δ, a topological transition is driven, separating a semi-metallic phase with two Dirac points and a gapped phase. We have calculated analytically several quantities, such as the density of states, the specific heat, and the integrated density of states related to the area of semiclassical orbits. From this quantity, we obtain a simple semiclassical description of the Landau levels spectrum in a magnetic field B. More quantitatively, the problem in a magnetic field is related to a one-dimensional Schrödinger equation with a double well potential, whose potential barrier depends on the parameter Δ and the magnetic field B as $\Delta/B^{3/2}$. The spectrum of Landau levels scales as $\epsilon_n \propto B^{2/3} f_n(\Delta/B^{3/2})$. In the vicinity of the topological transition, it is very well described by the Bohr-Sommerfeld quantization rule $S(\epsilon)\ell_B^2 = 2\pi(n + 1/2)$.

This Hamiltonian is appropriate to describe continuously the coupling between valleys which is usually neglected in the case of graphene, but which becomes important when approaching the topological transition. During completion of this paper, we have been aware of similar results in reference [29].

References

1. P.R. Wallace, Phys. Rev. **71**, 622 (1947)
2. For a review see A.H. Castro Neto, F. Guinea, N.M.R. Peres, K.S. Novoselov, A.K. Geim, Rev. Mod. Phys. **81**, 109 (2009)
3. Y. Hasegawa, R. Konno, H. Nakano, M. Kohmoto, Phys. Rev. B **74**, 033413 (2006)
4. P. Dietl, F. Piéchon, G. Montambaux, Phys. Rev. Lett. **100**, 236405 (2008)
5. V.M. Pereira, A.H. Castro Neto, N.M.R. Peres, Phys. Rev. B **80**, 045401 (2009)
6. B. Wunsch, F. Guinea, F. Sols, New J. Phys. **10**, 103027 (2008)
7. G. Montambaux, F. Piéchon, J.-N. Fuchs, M.O. Goerbig, Phys. Rev. B **80**, 153412 (2009)
8. O. Bahat-Treidel, O. Peleg, M. Grobman, N. Shapira, T. Pereg-Barnea, M. Segev, `http://arxiv.org/abs/0905.4278`
9. G.E. Volovik, Lect. Notes Phys. **718**, 31 (2007)
10. S. Katayama, A. Kobayashi, Y. Suzumura, J. Phys. Soc. Jap. **75**, 054705 (2006)
11. A. Kobayashi, S. Katayama, Y. Suzumura, H. Fukuyama, J. Phys. Soc. Jap. **76**, 034711 (2007)

12. M.O. Goerbig, J.N. Fuchs, F. Piéchon, G. Montambaux, Phys. Rev. B **78**, 045415 (2008)
13. S.-L. Zhu, B. Wang, L.-M. Duan, Phys. Rev. Lett. **98**, 260402 (2007)
14. E. Zhao, A. Paramekanti, Phys. Rev. Lett. **97**, 230404 (2006)
15. J.-M. Hou, W.-X. Yang, X.-J. Liu, Phys. Rev. A **79**, 043621 (2009)
16. K.L. Lee, B. Gremaud, R. Han, B.-G. Englert, C. Miniatura, Phys. Rev. A **80**, 043411 (2009)
17. J.W. McClure, Phys. Rev. **104**, 666 (1956)
18. D. Hofstadter, Phys. Rev. B **14**, 2239 (1976)
19. R. Rammal, J. Physique **46**, 1345 (1985)
20. Y. Hasegawa, M. Kohmoto, Phys. Rev. B **74**, 155415 (2006)
21. S. Banerjee, R.R.P. Singh, V. Pardo, W.E. Pickett, Phys. Rev. Lett. **103**, 016402 (2009)
22. We consider here the case where there is only one pair of Dirac points, although the number of pairs may be larger than one: F. Piéchon et al., in preparation
23. We stress that the $x-y$ directions define local axes which are fixed by the band parameters t_{mn}
24. Note that there are many equivalent ways of writing such an Hamiltonian using global $SU(2)$ transformations
25. L. Onsager, Phil. Mag. **43**, 1006 (1952); I.M. Lifshitz, A.M. Kosevich, Sov. Phys. JETP **2**, 636 (1956)
26. I.S. Gradshteyn, I.M. Ryzhik, A. Jeffrey, *Tables of integrals, series, and products* (Academic Press, 2007)
27. This corrects a slight mistake in reference [7]
28. G.P. Mikitik, Yu.V. Sharlai, Phys. Rev. Lett. **82**, 2147 (1999)
29. K. Esaki, M. Sato, M. Kohmoto, B.I. Halperin, Phys. Rev. B **80**, 125405 (2009)